Dehydriding process of α-AlH3 observed by transmission electron microscopy and electron energy-loss spectroscopy

doi: 10.1063/1.3151958

Dehydriding process of α-AlH_3 observed by transmission electron microscopy and electron energy-loss spectroscopy

S. Muto,[1,a] K. Tatsumi,[1] K. Ikeda,[2] and S. Orimo[2]
[1]*Department of Materials, Physics and Energy Engineering, Graduate School of Engineering, Nagoya University, Nagoya 464-8603, Japan*
[2]*Institute for Materials Research, Tohoku University, Sendai 980-8577, Japan*

(Received 29 April 2009; accepted 12 May 2009; published online 19 June 2009)

The dehydriding reaction of α-AlH_3 induced by high-energy electron irradiation was observed *in situ* by transmission electron microscopy and associated electron energy-loss spectroscopy (EELS). An α-AlH_3 crystal decomposed into fine aluminum particles while retaining its initial external shape because of a thin rigid surface layer that covered the entire particle. EELS revealed that the thin surface layer was amorphous aluminum oxide, which stabilizes α-AlH_3 particles at ambient temperature. © *2009 American Institute of Physics*. [DOI: 10.1063/1.3151958]

I. INTRODUCTION

Aluminum trihydride (AlH_3, alane) is a promising material for storing hydrogen. It has been intensively investigated because of its high gravimetric density (10 mass %) and volumetric hydrogen density (149 kg H_2/m^3), as well as its simple dehydriding reaction ($AlH_3 \rightarrow Al + 3/2H_2$) that occurs in a relatively low temperature range (370–470 K).[1–3] α-AlH_3 is the most stable phase among all the reported crystalline structures of AlH_3.[4] It exhibits an enthalpy change associated with the dehydriding reaction in the range of −5.7 to −7.6 kJ/mol H_2,[3,5,6] corresponding to an equilibrium hydrogen pressure of AlH_3 of around 1 GPa at 298 K. This suggests the presence of a surface protecting layer on AlH_3 particles, which prevents the dehydriding reaction of AlH_3 to Al from occurring at room temperature.[5–9] There have been several reports on the size and morphology of AlH_3 observed by scanning electron microscope (SEM),[10] though detailed observations of the internal structures are very few. Beattie *et al.*[11] reported *in situ* transmission electron microscopy (TEM) observations of thermal desorption of alane ethereal intermediate ($AlH_3 \cdot n Et_2O$). However, no reliable surface analysis of AlH_3 particles has been reported because it is difficult to apply electron microscopic techniques due to the unstable nature of AlH_3 particles under high-energy electron irradiation. The ethereal intermediate phase seemed quite stable for electron irradiation, which allowed Beattie *et al.* to *in situ* observe the removal of the ether solvent from the ethereal intermediate,[11] but they actually mentioned that the solvent free AlH_3 phase decomposed within seconds on exposure to the electron beam. They do not show a TEM image nor electron diffraction (ED) pattern of *pure* α-AlH_3 phase.

Recently, we solved the above problem and reported TEM observations of the dehydriding reaction process of AlH_3 under very low electron doses.[12] In the present paper, we extend the previous preliminary report of the dehydriding process by giving a detailed chemical analysis of AlH_3 by electron energy-loss spectroscopy (EELS) by using a spectrometer attached to the transmission electron microscope. We examined the plasmon loss and core-electron excitation spectra. The plasmon loss is useful for identifying individual phases and the decomposition process because of its strong intensity. The electron energy loss near edge structure (ELNES) in the core-electron excitation spectrum reflects the density of states of the excited atom, which is very sensitive to the nature of the local chemical bonding.

II. EXPERIMENTAL

AlH_3 particles were prepared by the chemical reaction between $LiAlH_4$ and $AlCl_3$ in an ether (99.5% purity Et_2O) solution.[3,6,13,14] The particles were then examined by thermogravimetric analysis (heating rate of 1 K/min under He) and powder x-ray diffraction measurements (Cu $K\alpha$ radiation) to confirm that the particles consisted of the single α-AlH_3 phase. The obtained particles were dispersed on a carbon microgrid mesh, the entire processes of which were done in a glove box (dew point <183 K, oxygen concentration <1 ppm) without exposure to air. The sample grid mesh was transferred to a TEM (JEOL JEM2100 S/TEM with a Gatan ES500W Erlangshen charge-coupled device high-speed camera and Enfina 1000 EELS) for *in situ* TEM-EELS observations. The transfer process involved brief exposure to the atmosphere, though we confirmed that the present sample exhibited no appreciable change in the hydrogen desorption property after such brief exposure to air.[12] The *in situ* TEM observations were carried out at 100 kV under an electron flux of approximately 2×10^5 electrons/nm^2 s; this low electron flux ensured that no fast damage was caused to the particles due to electron irradiation. The maximum energy transfer by electron irradiation to the aluminum atoms was estimated to be approximately 9 eV [870 kJ/mol Al], which is still sufficiently large to decompose AlH_3 [5.7–7.6 kJ/mol H_2 (or 8.6–11.4 kJ/mol Al)].

The experimental ELNES data were compared with theoretical ELNES results calculated by the orthogonalized linear combination of atomic orbitals method with local approximation to density functional theory.[15] Supercells consisting of 125, 216, 120, and 112 atoms with one core-hole Al were used for Al, AlH_3, Al_2O_3, and $Al(OH)_3$, respec-

[a]Electronic mail: s-mutoh@nucl.nagoya-u.ac.jp.

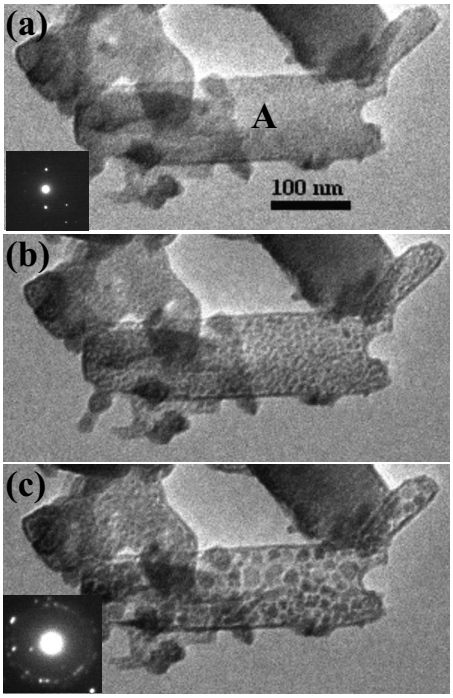

FIG. 1. Low-dose TEM observations of the dehydriding process of AlH_3 particles. Selected area diffraction patterns from particle A are shown in the insets in (a) and (c). Each photograph was taken on an exposure of 5 s.

tively. Prior to the spectral calculations, the crystal parameters of the structures were fully optimized using a different first-principles procedure, the projected augmented-wave method,[16,17] in order to reduce the computational cost. For the spectral calculations, the transition probabilities of the Al $2p$ excitations were calculated within the electric-dipole approximation. These were integrated into the whole Brillouin zone of the supercell using a $2\times2\times2$ k-point mesh. The final spectrum was broadened by convoluting it with a Gaussian function with a full width at half maximum (FWHM) of 1.2 eV.

III. RESULTS AND DISCUSSION

A series of TEM images of the dehydriding process is shown in Fig. 1. The AlH_3 particles were initially single crystals and they subsequently decomposed into an assembly of nanoparticles. It should be noted that electron illumination onto the sample with a current density necessary for usual observation instantly decomposed the sample particles. The TEM images show that the initial particle shape remained unchanged during the dehydriding process; they also reveal a thin surface layer, as has been reported, based on SEM observations.[10] The x-ray photoelectron spectroscopy (XPS) analysis[12] of the as-prepared sample powder unexposed to air clearly revealed the presence of oxygen in the surface regions, where no significant change in the relative oxygen concentration was observed with respect to the x-ray incident angle. This suggests that surface oxide layers with a few nanometers were already formed during the material synthesis, rather than formed during the sample transfer to the TEM.

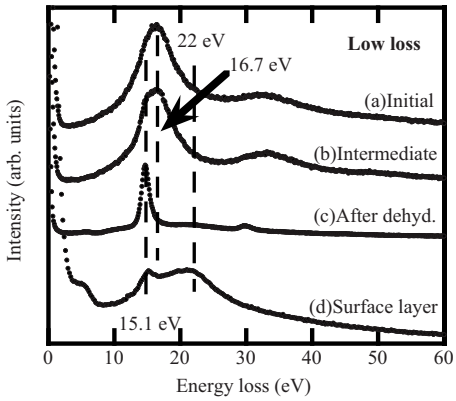

FIG. 2. EEL spectra of the low loss region from [(a)–(c)] particle A corresponding to Figs. 1(a)–1(c) and from (d) the surface layer after dehydrogenation.

The ED pattern for a fully dehydrided particle [indicated by A in Fig. 1(a)] exhibited Debye rings, consistent with a fcc structure. Unfortunately, an ED pattern from the initial state could not be obtained from a low-order zone axis so that we were unable to fully ensure that the particle was α-AlH_3. We checked all the other possible phases besides α-AlH_3 (such as β-, γ-, and α'-AlH_3) even though none of them could consistently explain the ED pattern of the initial state. We also examined the possibility of $Al(OH)_3$ because we were concerned that the AlH_3 phase could deteriorate by absorbing ambient moisture during transfer of the sample into the TEM. We confirmed that the ED pattern of the initial phase was not consistent with $Al(OH)_3$.

The corresponding low-loss spectra are shown in Fig. 2, where spectra (a)–(c) were obtained from particle A in Figs. 1(a)–1(c), respectively. The exposure time for a single acquisition was 0.1 s with an energy dispersion of 0.1 eV/channel. The FWHM of the zero-loss peak was 1.1 eV. The distinct peaks around 15–17 eV are volume plasmon peaks, each peak corresponding to a single phase. The broad peak at 16.7 eV was gradually replaced by the sharp peak at 15.1 eV during dehydriding. The 15.1 eV plasmon peak coincides with the reference spectrum of metallic Al, which is consistent with the TEM and ED results in Fig. 1. The plasmon energy, E_p, can be theoretically predicted by the equation

$$E_p = \hbar\sqrt{\frac{ne^2}{\varepsilon_0 m}}, \tag{1}$$

where $\hbar = h/2\pi$, h is Planck's constant, n is the valence electron density, e is the electron charge, ε_0 is the dielectric constant of vacuum, and m is the electron mass. Assuming that metallic Al is monovalent and that Al in α-AlH_3 is trivalent, $E_p(\alpha\text{-}AlH_3)$ is estimated to be 17.1 eV, which is in reasonable agreement with the experimental value of 16.7 eV. Hence, the initial phase is likely to be α-AlH_3.

Since it was not possible to use the ED pattern to identify whether the initial phase was α-AlH_3, element-selective core-electron spectroscopy was used instead. The Al $L_{2,3}$ ELNES starting at around 70 eV was extracted from each low-loss spectrum in Figs. 2(a) and 2(c), as shown in Fig. 3(a), together with the reference spectra for metallic Al, α-Al_2O_3, and amorphous alumina.[18] Since the signal-to-noise ratio of

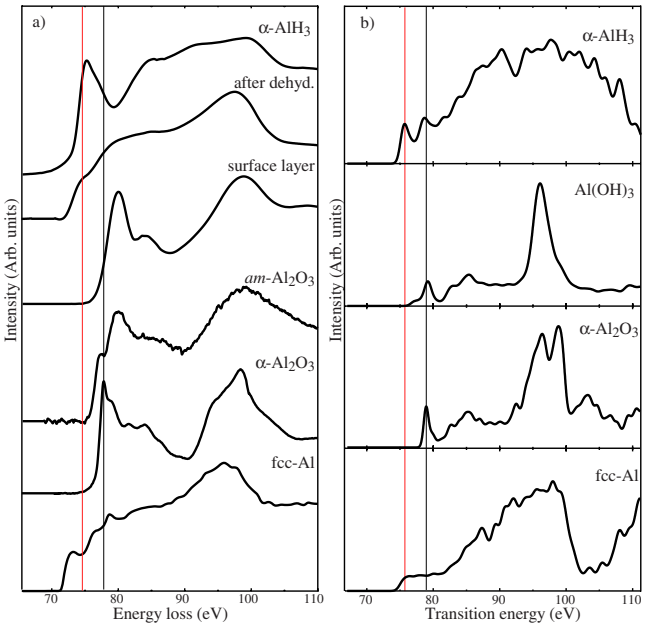

FIG. 3. (Color online) (a) (From top to bottom) Experimental Al $L_{2,3}$ ELNES acquired from a particle in the initial state and after dehydrogenation, from the surface layer and three possible reference phases from a database. (b) Theoretical Al $L_{2,3}$ ELNES for several Al-related phases. Theoretical transition energy is shifted by +1.6 eV so that the first peak of the theoretical spectrum for Al $L_{2,3}$ of α-Al_2O_3 is aligned with that of the corresponding experimental spectrum.

the Al $L_{2,3}$ ELNES spectra was very low (<5), the spectra were processed by the Pixon method[19] to restore the spectral profiles and to effectively remove statistical noise after subtracting the pre-edge background by a power law.

The Al $L_{2,3}$ ELNES of the dehydrided phase coincides with the reference spectra of metallic Al, which is consistent with the ED observation. The Al $L_{2,3}$ ELNES of the initial state is characterized by a distinct peak at the onset of the spectrum and no significant chemical shift of the threshold, neither of which coincide with the spectral features of metallic Al or aluminum oxides. Therefore, we compared the experimental and theoretical ELNES data [the latter is shown in Fig. 3(b)]. Even though the intensities at the lower energy side of the theoretical spectral tend to be systematically underestimated compared to those of the experimental spectra, the peak profiles, positions, and chemical shifts of the threshold for the experimental and theoretical ELNES for metallic and α-Al_2O_3 are in reasonable agreement. The observed chemical shift again excluded the possibility of $Al(OH)_3$. The unknown ELNES from the particle in the initial state also shows plausible agreement with the theoretical spectra of α-AlH_3. We can therefore safely conclude that the initial phase is the α-AlH_3 phase and that we successfully observed *in situ* the dehydriding process of α-AlH_3, both microscopically and spectroscopically. The 16.7 eV plasmon peak can thus be used as a fingerprint of the α-AlH_3 phase.

Although it was hard to acquire EELS core loss spectra from the particle before dehydrogenation due to its instability under electron irradiation, it was possible to record sufficient counts from the particles after dehydrogenation. The surface layer thickness was estimated to be 3–7 nm from Fig. 1, and a ~5 nm diameter electron probe in the scanning

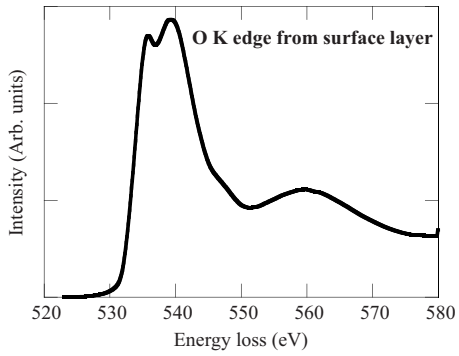

FIG. 4. Experimental O *K* ELNES acquired from the surface layer of the particle after dehydrogenation.

TEM mode was placed on the surface layer to acquire the EELS spectra. The low loss spectra including the Al $L_{2,3}$ ELNES and O *K* ELNES were recorded. The low loss part and Al $L_{2,3}$ ELNES are also shown in Figs. 2(d) and 3(a), respectively, and the O *K* ELNES is shown in Fig. 4. Pixon signal processing was also applied to the core loss spectra.

The low loss spectrum exhibits a broad plasmon peak at around 22 eV with a small shoulder peak at 15.1 eV, presumably from the adjacent metallic Al particles. Aluminum oxide is a possible candidate for the surface layer, and actually amorphous alumina has been reported to have a broad plasmon peak at 21–22 eV.[20] The Al $L_{2,3}$ and O *K* spectral profiles agree with the reference spectra of amorphous alumina (the O *K* reference spectrum is given in Ref. 21). We also detected a small amount of carbon in the surface layer, which is consistent with the XPS analysis.[12]

Finally, since electron irradiation directly deposits energy into the target material, we examined whether the dehydriding process by electron irradiation is the same as thermal decomposition. We did this by preparing a sample in the same way as described above. It was placed in the specimen heating holder and heated to 430 K at an approximate heating rate of 10 K/min. The initial and final states of AlH_3 particles after thermal decomposition without electron irradiation are shown in Figs. 5(a) and 5(b), respectively. During heating, the AlH_3 particles of interest were moved out of the field of view to avoid electron irradiation and they were then returned to the field of view when the temperature reached 430 K. The morphology of the final state is very similar to that produced by electron irradiation: metallic Al nanoparticles were formed with their external shape almost unchanged because of the surface protecting layers. Thus, the electron irradiation-induced dehydriding process observed above is considered to be similar to that of thermal decomposition. On closer inspection of many decomposed particles, we noted that the Al particle size distribution tends to be more homogeneous for the nanoparticles produced by electron irradiation than that for the nanoparticles produced by thermal decomposition. This is probably because the homogeneous electron irradiation resulted in more homogeneous decomposition, suggesting that the dehydriding reaction proceeds as a simple nucleation and growth mechanism.

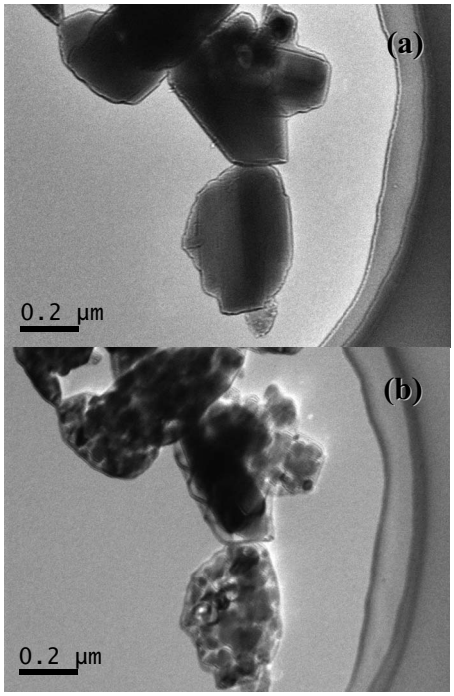

FIG. 5. TEM images of (a) initial and (b) final states of AlH_3 particles after thermal decomposition without electron irradiation.

IV. SUMMARY

We successfully observed the electron-irradiation-induced dehydriding process of AlH_3 by TEM and EELS. A single crystal of AlH_3 was decomposed into metallic Al nanoparticles, while the external shape remained almost unchanged. The experimental Al $L_{2,3}$ spectrum of the initial state showed good agreement with the theoretical spectrum of α-AlH_3; this will be important for discussing the nature of the Al–H chemical bonding and for improving the hydrogen storage characteristics AlH_3. The EELS results confirmed that the surface layer covering the AlH_3 particle was thin amorphous alumina with a thickness of 3–5 nm. Electron irradiation-induced dehydrogenation is considered to proceed in a similar way to thermal decomposition since the morphologies of the final states are very similar to each other.

ACKNOWLEDGMENTS

This work was supported in part by Grants-in-Aid for Scientific Research (KAKENHI) on Priority Areas (#474) "Atomic Scale Modification" and Houga-kenkyu (Grant No. 20656102) from the Ministry of Education, Culture, Sports, Science and Technology (MEXT), Japan and the seeds innovation project from the Japan Science and Technology Agency. One of the authors (K.I.) was supported by a grant from the Yazaki Memorial Foundation for Science and Technology.

[1]G. Sandrock, J. Reilly, J. Graetz, W.-M. Zhou, J. Johnson, and J. Wegrzyn, Appl. Phys. A: Mater. Sci. Process. **80**, 687 (2005).
[2]J. Graetz and J. J. Reilly, J. Phys. Chem. B **109**, 22181 (2005).
[3]S. Orimo, Y. Nakamori, T. Kato, C. Brown, and C. M. Jensen, Appl. Phys. A: Mater. Sci. Process. **83**, 5 (2006).
[4]F. M. Brower, N. E. Matzek, P. F. Reigler, H. W. Rinn, C. B. Roberts, D. L. Schmidt, J. A. Snover, and K. Terada, J. Am. Chem. Soc. **98**, 2450 (1976).
[5]C. Wolverton, V. Ozoliš, and M. Asta, Phys. Rev. B **65**, 144109 (2004).
[6]X. Ke, A. Kuwabara, and I. Tanaka, Phys. Rev. B **71**, 184107 (2005).
[7]H. W. Brinks, A. Istad-Lem, and B. C. Hauback, J. Phys. Chem. B **110**, 25833 (2006).
[8]H. Saitoh, A. Machida, and K. Aoki, Appl. Phys. Lett. **93**, 151918 (2008).
[9]R. H. Scheicher, D. Y. Kim, S. Lebéque, B. Amaud, M. Alouani, and R. Ahuja, Appl. Phys. Lett. **92**, 201903 (2008).
[10]For example, P. J. Herley and R. H. Irwin, J. Phys. Chem. Solids **39**, 1013 (1978), and several scientific meetings in 2004–2005 by G. Sandrock *et al.*
[11]S. D. Beattie, T. Humphries, L. Weaver, and G. S. McGrady, Chem. Commun. (Cambridge) **2008**, 4448.
[12]K. Ikeda, S. Muto, K. Tatsumi, M. Menjo, S. Kato, M. Bielman, A. Züttel, C. M. Jensen, and S. Orimo, Nanotechnology **20**, 204004 (2009).
[13]P. Claudy, B. Bonnetot, and J. M. Letoffe, J. Therm. Anal. **15**, 129 (1979).
[14]T. Kato, Y. Nakamori, S. Orimo, C. Brown, and C. M. Jensen, J. Alloys Compd. **446–447**, 276 (2007).
[15]W. Y. Ching, J. Am. Ceram. Soc. **73**, 3135 (1990).
[16]G. Kresse and J. Furthmüller, Phys. Rev. B **54**, 11169 (1996).
[17]G. Kresse and D. Joubert, Phys. Rev. B **59**, 1758 (1999).
[18]The EELS data base: http://www.cemes.fr/~eelsdb/index.php?page=search.php.
[19]S. Muto, R. C. Puetter, and K. Tatsumi, J. Electron Microsc. **55**, 215 (2006).
[20]B. Rufino, F. Boulc'h, M.-V. Coulet, G. Lacroix, and R. Denoyel, Acta Mater. **55**, 2815 (2007).
[21]C. Scheu, J. Microsc. **207**, 52 (2002).